

STP 1597, 2018 / available online at [www.astm.org](http://www.astm.org) / doi: 10.1520/STP159720160052

M. Nedim Cinbiz,<sup>1</sup> Arthur T. Motta,<sup>1</sup> Donald Koss,<sup>2</sup>  
and Michael Billone<sup>3</sup>

## Hydride Reorientation in Zircaloy-4 under Different States of Stress as Studied with In Situ X-Ray Diffraction

### Citation


Cinbiz, M. N., Motta, A. T., Koss, D., and Billone, M., "Hydride Reorientation in Zircaloy-4 under Different States of Stress as Studied with In Situ X-Ray Diffraction," *Zirconium in the Nuclear Industry: 18th International Symposium, ASTM STP1597*, R. J. Comstock and A. T. Motta, Eds., ASTM International, West Conshohocken, PA, 2018, pp. 1252-1285, <http://dx.doi.org/10.1520/STP159720160052><sup>4</sup>

### ABSTRACT

Hydride reorientation can occur as a result of vacuum drying or transportation of spent nuclear fuel rods prior to dry cask storage. The elevated temperatures generate high internal gas pressure in the fuel rods, causing  $\delta$ -hydride platelets to precipitate perpendicular to the hoop stress during cooling. Because the loading causes multiaxial stresses, it is of interest to elucidate the role of stress state on the threshold stress for hydride reorientation. To that end, specially designed specimens were used with a range of stress biaxiality ratios ( $\sigma_1/\sigma_2$ ) from uniaxial tension ( $\sigma_1/\sigma_2 = 0$ ) to near-equibiaxial tension ( $\sigma_1/\sigma_2 = 0.8$ ). The threshold stress was determined in each case by matching the major and minor stresses (and thus the local stress state) calculated by finite-element analysis to the hydride microstructures created by the thermomechanical treatment at that specific location. Using cold-worked stress-relieved Zircaloy-4, the results show that as the stress biaxiality ratio increased from uniaxial tension to near-equibiaxial tension, the threshold stress decreased from 155 to 75 MPa. To elucidate the

---

Manuscript received February 29, 2016; accepted for publication August 15, 2016.

<sup>1</sup>Pennsylvania State University, Dept. of Mechanical and Nuclear Engineering, 138 Reber Bldg., University Park, PA 16802 M. C.  <http://orcid.org/0000-0003-4626-8515>

<sup>2</sup>Pennsylvania State University, Dept. of Materials Science and Engineering, University Park, PA 16802

<sup>3</sup>Argonne National Laboratory, Nuclear Engineering Division, Argonne, IL 60439

<sup>4</sup>ASTM 18th International Symposium on *Zirconium in the Nuclear Industry* on May 15-19, 2016 in Hilton Head, SC.

Copyright © 2018 by ASTM International, 100 Barr Harbor Drive, PO Box C700, West Conshohocken, PA 19428-2959.

hydride reorientation process, hydride precipitation and d-spacing behavior were investigated in situ using synchrotron radiation diffraction. The precipitation temperature for out-of-plane hydrides was lower than that for in-plane hydrides. The  $\delta\{111\}$  d-spacing aligned with the hydride platelet face was greater than the d-spacing of planes aligned with platelet edges. Furthermore,  $\delta\{111\}$  planes exhibited bilinear thermally induced expansion, but only for those planes aligned with hydride plate edges. In contrast, the hydride platelet face contracted upon heating. The experimental results were explained by a reversal of stress state associated with precipitating or dissolving hydrides within  $\alpha$ -zirconium. In addition, irradiated cladding after thermomechanical treatments was examined by synchrotron radiation diffraction at ambient temperatures. Although the hydride intensity was low for accurately determining d-spacing, the diffraction patterns indicated that  $\beta$ -niobium peaks present in the un-irradiated cladding were diminished after irradiation.

### Keywords

synchrotron radiation, hydride, zirconium, threshold stress, in situ X-ray diffraction, stress state, biaxiality ratio, Zircaloy-4, hydride reorientation, irradiated cladding

## Introduction

During nuclear reactor operation, hydrogen is picked up by the cladding as a result of waterside corrosion of the zirconium alloy. When the solid solubility limit of hydrogen in the alloy is exceeded [1,2], hydrogen precipitates as circumferential (in-plane)  $\delta$ -hydride platelets, i.e., with faces perpendicular to the radial direction of the cladding tube (equivalent to the normal direction of sheet samples), as primarily caused by the crystallographic texture. Spent fuel rods may be subjected to a heat treatment to remove moisture from the outer surface prior to dry storage or transportation. During the heat-up stage of vacuum drying, the internal pressure within the cladding tubes increases because of the expansion of fill gases and gaseous fission products, giving rise to multiaxial tensile stresses. Although the hydrides partially or entirely dissolve in the cladding at the elevated temperatures required for drying (up to 400°C), the subsequent cool down causes hydride reprecipitation. It is well known that if hydrogen precipitation from a solid solution occurs under a sufficiently high hoop stress component (i.e., above a threshold stress), hydride reorientation occurs in which radial (out-of-plane) hydride platelets precipitate and then are oriented perpendicular to the hoop stress [3–6]. These radial hydrides can drastically degrade the mechanical response of the cladding tube by changing the failure mode at low temperatures from ductile to brittle-like such that a through-thickness crack can much more easily propagate [7–10]. The change in failure mode is accompanied by an increase in the ductile-to-brittle transition temperature of the cladding even at relatively low hydrogen concentrations [8,10]. The subsequent performance and retrievability of the spent

fuel cladding under transport and storage conditions could be adversely affected as a result.

Hydride reorientation is influenced by properties inherent to the alloy such as the amount of cold work, grain microstructure, and crystallographic texture [3,4,11–14]. In addition, the specific influences of thermomechanical parameters such as maximum temperature, dwell time at maximum temperature, cooling rate and number of cycles, and applied stress on the threshold stress for hydride reorientation have been extensively studied [8,9,15–19]. However, although there is a significant amount of data on the value of the threshold stress to reorient the hydrides during cooling, most of it was obtained under uniaxial tension conditions [4,6,12,17,20–24], whereas the internal gas pressure creates biaxial stress states with stress biaxiality ratios ( $\sigma_2/\sigma_1 \approx 0.5$ ) that are significantly higher than uniaxial tension ( $\sigma_2/\sigma_1 = 0$ ). Some threshold stress data for hydride reorientation are available from studies using internally pressurized tubes that produce stress states similar to what occurs during vacuum drying [9,15,16]; however, these values vary widely, making a firm comparison to the many threshold stress values obtained from uniaxial testing difficult. Thus, the effect of the stress state on the threshold stress to reorient hydrides in cladding material is not well known because no systematic study has addressed this issue to date. Furthermore, it is of interest to understand the mechanism of hydride reorientation in detail. One possible approach is to use high-energy synchrotron radiation diffraction to study the changes in the hydride diffraction peaks during a thermomechanical treatment while the sample is subjected to load at temperature. Using this method, it is possible not only to follow the diffracted intensity of the sample in situ but also the change in the lattice parameter as the hydrides dissolve and reprecipitate with and without load. By separately integrating the different orientations of the diffraction ring, it is possible to obtain diffraction signals from the planes oriented along the load direction or perpendicular to it and thus from the face or the edge of the hydride particles. Although recent studies have utilized high-energy synchrotron radiation to examine the hydride dissolution/precipitation behavior in situ during the thermal cycling behavior of zirconium alloys [25–30], several aspects of the observed d-spacing behavior of hydride planes are not only complex but also poorly understood. For example, although the existence of a radial hydride signature has been identified [24], the root cause of this signature has not been explained.

This study examined the role of the stress state on hydride reorientation and the d-spacing behavior of both in- and out-of-plane hydrides during thermomechanical treatment. The threshold stress to reorient hydrides was determined using specimen configurations that produced stress states ranging from uniaxial tension ( $\sigma_2/\sigma_1 = 0$ ) to near-equal biaxial tension ( $\sigma_2/\sigma_1 \approx 0.8$ ) that bound the conditions of vacuum drying. High-energy synchrotron radiation diffraction data were analyzed for d-spacing behavior because both in- and out-of-plane hydrides dissolve and precipitate during thermomechanical treatment under a multiaxial stress state

similar to that of cladding undergoing a drying cycle. The results and its implications were analyzed and discussed in the context of the known literature.

## Experimental Methods

This study utilized cold-worked stress-relieved (CWSR) Zircaloy-4 flat sheet material with a nominal thickness of 0.67 mm that was obtained from ATI Specialty Alloys and Components. This Zircaloy-4 sheet exhibited the usual strong crystallographic texture [31] with basal planes that were aligned  $\pm 30^\circ$  away from the sheet normal along the transverse direction (TD) [32]. Kearns factors [3] of the sheet in three different directions were measured as  $f_N = 0.59$ ,  $f_L = 0.05$ , and  $f_T = 0.31$  in the normal direction, rolling (similar to longitudinal) direction (RD), and TD, respectively [33], similar to a typical CWSR Zircaloy-4 nuclear fuel cladding tube texture [34].

Hydriding of the samples was performed by gaseous diffusion. Prior to the hydriding process, the native oxide layer was removed using an acid solution of distilled water, nitric acid, and hydrofluoric acid by parts in volume 10:10:1, following which the samples were coated with a 200-nm-thick nickel layer to allow hydrogen diffusion into the samples. The samples were then heated in a tube furnace to 500°C under a vacuum of less than 13.3  $\mu\text{Pa}$ , and a mix of hydrogen and argon gas (12.5 %  $\text{H}_2$  and 87.5 % Ar by volume) was introduced for 2 h at 500°C. This treatment simultaneously induced hydrogen absorption, homogenization, and stress relief. The hydrogen contents of the samples were approximately 180 wt. ppm (maximum: 197 wt. ppm; minimum: 157 wt. ppm); these contents were systematically determined before and after thermomechanical treatment using hot-vacuum extraction<sup>5</sup> [35]. The hydrogen level of 180 wt. ppm was high enough that precipitation during cooling started at a temperature at which hydrogen is mobile and low enough that the complete dissolution of hydrogen can occur at a reasonable temperature (approximately 400°C).

The uniaxial tensile behavior of this CWSR Zircaloy-4 sheet was determined previously for temperatures ranging from 25 to 400°C [24,36–39]. For example, the yield stress at room temperature was 600 MPa, and at 400°C, which was the assumed temperature of the finite-element analyses of the specimens, it was 300 MPa. In addition, at 400°C, the strain-hardening exponent had the following value:  $n = d \ln \sigma / d \ln \epsilon = 0.022$ .

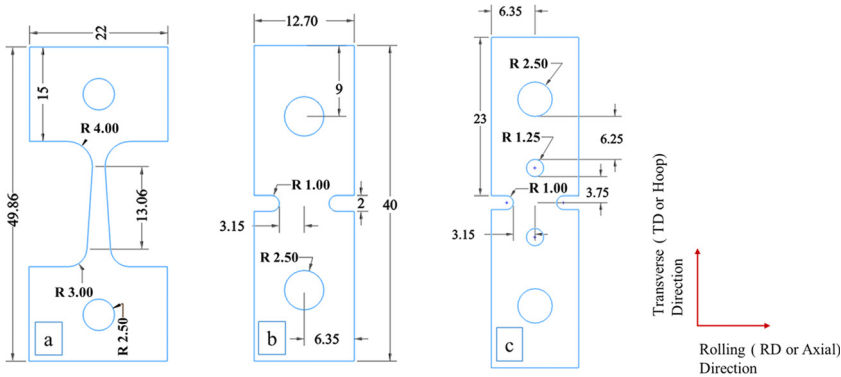
Fig. 1 shows the three types of test specimens used to create the range of stress states: tapered uniaxial, plane strain [37,40], and near-equibiaxial. The tensile axes of these specimens were oriented along the TD (corresponding to the hoop orientation of a cladding tube).

Because the double-edge notched-based geometry requires numerical calculations to determine stress distributions within the samples, finite element analyses were

---

<sup>5</sup>For the samples that were utilized to determine threshold stress values, the hydrogen contents over the sample length and width before thermomechanical treatment showed differences of less than 10 wt. ppm. After the thermomechanical treatment, we did not observe a difference in hydrogen content more than 15 wt. ppm within the sample gage section and over the gage length.

**FIG. 1** Mechanical test specimen geometries (all dimensions shown are in mm): (a) tapered uniaxial tension, (b) plane-strain double-edge notch tension, and (c) near-equibiaxial double-edge notch specimen with holes. The mechanical load was applied along the TD that corresponds to the hoop direction for tube geometry. TD = transverse direction.



performed using ANSYS to calculate the magnitude of the local principal stresses along with the corresponding stress biaxiality ratios. These calculations were performed under the assumptions of plane stress through the thickness and isotropic<sup>6</sup> mechanical properties at 400°C. The finite element analysis performed on the plane-strain tension sample geometry in the elastic region indicated that the stress biaxiality ratio ( $\sigma_1/\sigma_2$ ) across the gage width decreased from 0.57 (near plane strain) at the mid-point between the two notches to 0 (uniaxial tension) near the notch. To investigate the stress-state effect for stress biaxiality ratios greater than 0.57, the near-equibiaxial samples shown in Fig. 1c were used. Fig. 2 shows plots of the major and minor stresses<sup>7</sup> and stress state along and perpendicular to the gage length. The notch and hole arrangement produces a range of biaxial stress states when under load. Near the center of the specimen, a near-equibiaxial stress biaxiality ratio of approximately 0.83 is achieved (see Fig. 2c). An extensive region exists near the gage center in which the major stress is nearly constant while the minor stress decreases, resulting in a range of stress states along the gage length. Although the finite element analysis predicts a small plastic zone near the notches of a loaded specimen, the threshold stress values reported later were determined from regions of the sample that remained elastic.

<sup>6</sup>Zircaloy-4 exhibits anisotropic mechanical properties; MATPRO reports approximately elastic moduli of 75 GPa along the axial and 72 GPa along the hoop directions at 400°C [41]. Because the difference in elastic moduli is small, we assumed the elastic modulus is isotropic at the hydride precipitation temperatures.

<sup>7</sup>Note that for these plane-stress analyses, the minimum principal stress was always the zero through-thickness stress. Thus, we adopted the notation for the in-plane stresses as the major and minor stresses; both are principal stresses, and the major stress is also the maximum principal stress.

**FIG. 2** Calculated stress-state response of the near-equibiaxial sample when the average tensile stress across the gage width (from one notch to another) was 210 MPa. (a, b) Major and minor stress distributions and the equivalent stress distribution; (c, d) stress biaxiality ratio along the gage width and length. The finite element calculation was performed using material properties at 375°C.

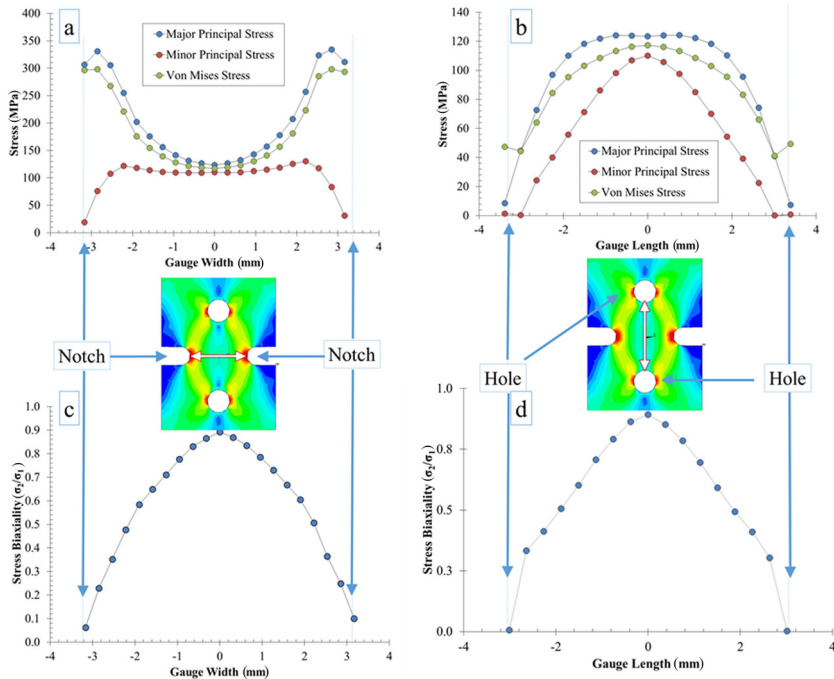
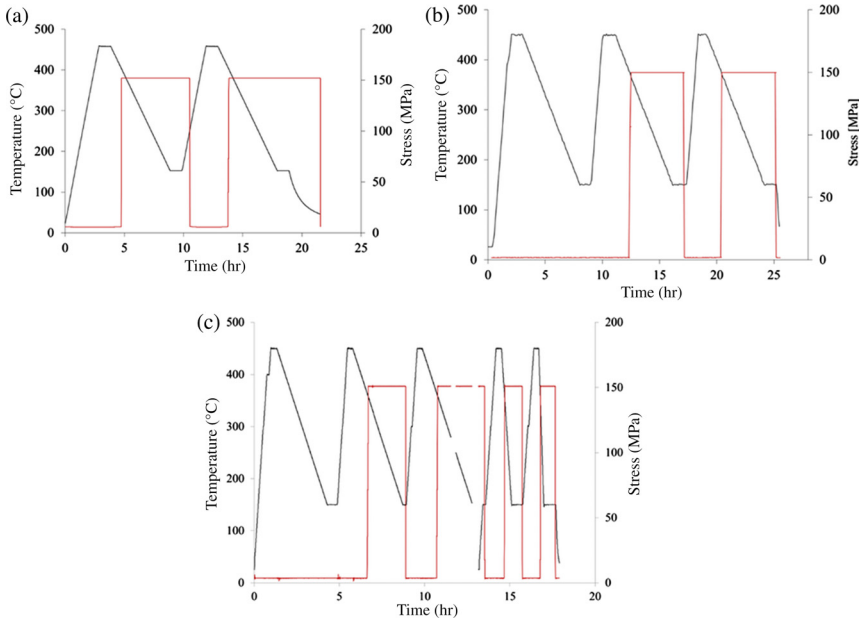


**Fig. 3** shows the two-, three-, and five-cycle thermomechanical treatment used in this study. Each cycle involved heating to 450°C (at a rate of 5°C/min) to dissolve the hydrides, a 1-h dwell, and subsequent cooling down to 150°C at a rate of 1°C/min, except for the fourth and fifth cycles in which the cooling rates were higher at 5 and 10°C/min. When the temperature reached 375°C (hydrogen still in solid solution) during cooling, a mechanical load was applied (red lines). The choice of 375°C was based on the desire to minimize any plastic zone near the specimen notches (due to increasing Zircaloy yield stress with decreasing temperatures) and yet to retain the hydrogen in solution. Subsequent cooling caused out-of plane hydride precipitation if the stress was higher than the threshold stress. The thermomechanical treatment shown in **Fig. 3b** and **c** were used in the in situ synchrotron radiation experiments; these treatments included a zero-stress first cycle to examine the dissolution and precipitation of in-plane hydride particles.

After the thermomechanical treatment, the hydride microstructures were characterized using light microscopy of either the normal plane, i.e., the flat sheet

**FIG. 3** Thermomechanical treatment (temperature in black and load in red) of samples for (a) ex situ bulk hydride reorientation experiments and in situ synchrotron radiation diffraction experiments: (b) three-cycle or (c) five-cycle thermomechanical treatment.



surface or through-thickness plane (normal to RD). For micrographs of the through-thickness plane, the degree of hydride reorientation was characterized using the radial hydride fraction (RHF), which was determined based on the examination of a 600 by 200- $\mu\text{m}^2$  rectangular region of the micrographs within which the ratio of total length of radially oriented hydrides to total length of all hydrides [31,42] was estimated as follows:

$$\text{RHF} = \frac{\text{Total length of hydrides oriented within } 45^\circ \leq \theta \leq 135^\circ}{\text{Total length of hydrides at any orientation}} \quad (1)$$

where:

$\theta$  = angular deviation from the TD of the sheet for the individual macroscopic hydrides [36].

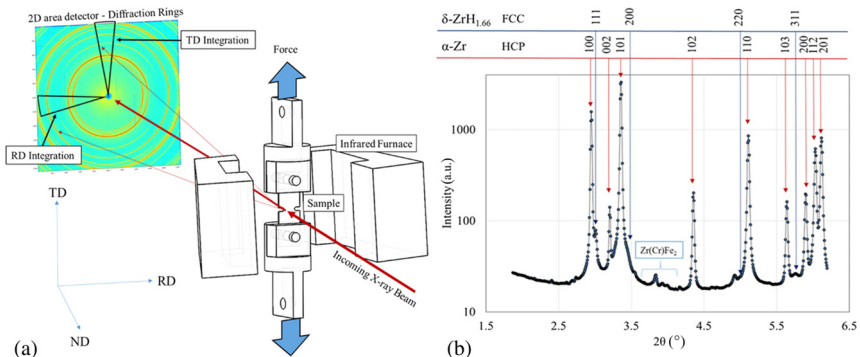
Using ImageJ software, hydrides were labeled according to their orientation, and their number and lengths were determined. For the through-thickness micrographs, the onset of hydride reorientation was defined as the achievement of a radial hydride fraction of 0.05.

Samples were examined after swab etching with the same solution used for the removal of the native oxide layer to reveal the hydrides. For micrographs that viewed the normal (or sheet surface) plane, the in-plane hydrides are oriented parallel to the plane of view and cannot be seen in these micrographs. However, the out-of-plane hydrides, which are perpendicular to the sheet surface, could be clearly seen after etching, and the onset of hydride reorientation was determined as occurring when the hydrides were first observed. The threshold stresses for hydride reorientation were identified as the calculated stresses by finite element analysis at that location.

In situ X-ray diffraction experiments were performed at the 1-ID-C beamline at the Advanced Photon Source at the Argonne National Laboratory. Fig. 4 shows the beamline experimental setup: a 100 by 100- $\mu\text{m}^2$  rectangular X-ray beam was incident on a sample that was placed in a furnace and subjected to load at temperature during the experiment. Because of its high energy (80 keV), the beam was transmitted through the 0.6-mm-thick double-edge notched sample that generated diffraction rings from both  $\alpha$ -zirconium and  $\delta$ -hydride phases that were recorded in an area detector. During hydride dissolution and precipitation, the diffraction data were continuously acquired by moving the incident beam sequentially to the locations on the sample where the stress biaxiality ratio was 0, 0.53, or 0.83. By integrating the diffraction rings over  $15^\circ$  arcs either aligned with the loading direction (TD) or normal to it (RD) [24,25], the hydride dissolution and precipitation behaviors were tracked in situ.

Fig. 4b shows the diffraction peaks after the integration of the ring patterns shown in Fig. 4a. These peaks were indexed and fitted using three types of software: pseudo-Voigt functions in GSAS [43] and MATLAB and the Pearson-7-Area function in Peak Fit [44]. The d-spacings, full-width at half maximum, and intensities of characteristic peaks of both zirconium and hydride phases could be determined.

**FIG. 4** (a) Experimental setup at the 1-ID-C beamline and (b) typical X-ray diffraction pattern of the sample integrated over the full diffraction ring as seen in (a) containing 172 wt. ppm hydrogen.



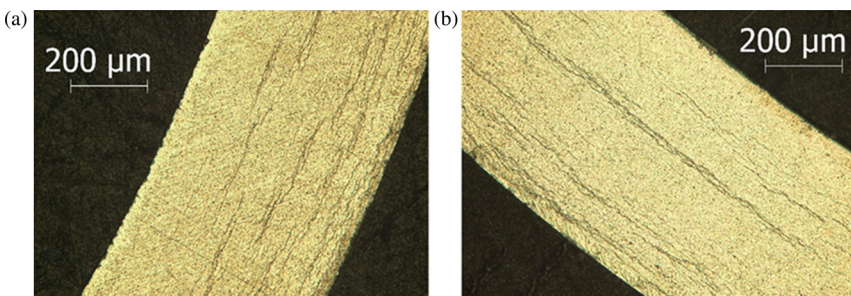


In the case of Fig. 4, the rings were integrated over the full circle, but the integration of segments along the RD or TD only are also possible.

To investigate the possible role of the radiation damage on hydride reorientation, two sets of irradiated cladding specimens, Zircaloy-4 and M5<sup>®</sup>, were examined using high-energy X-ray diffraction at ambient temperature. In the first experiment, irradiated cladding samples were prepared by cutting small slices of Zircaloy-4 from H. B. Robinson irradiated to a neutron fluence of  $14 \times 10^{25}$  neutrons/m<sup>2</sup> ( $E > 1$  MeV) for more than 6 years [45] and M5 cladding irradiated to a neutron fluence of  $14\text{--}16 \times 10^{25}$  neutrons/m<sup>2</sup> [46]. The inner and outer cladding surface oxide layers were removed by grinding and polishing, and metallography was performed on etched sister samples to characterize the hydride microstructure. The hydride microstructure of the as-irradiated Zircaloy-4 sister sample containing 270 wt. ppm hydrogen showed both a hydride rim and homogeneously distributed hydride platelets within the cladding (Fig. 5). These samples were examined in their as-irradiated state.

The preparation of the M5 samples was the same as the Zircaloy-4 samples. Prior to examination, each of the M5 samples was subjected to a single-cycle thermomechanical treatment with different levels of stress (Table 1) such that each specimen exhibited different levels of hydride reorientation. As shown in Table 1, the specimens had similar burnup values and hydrogen contents but different radial hydride continuity factors (RHCFs)<sup>8</sup> from 0 to 0.72 [8]. Fig. 6 shows that the initial microstructure of the as-irradiated sample (Sample 1) consisted primarily of circumferential hydrides with a few radial hydrides, whereas Fig. 7 shows the hydride microstructures with increasing levels of the RHCF. Increasing the applied stress from 90 to 140 MPa resulted in an RHCF increase from 31 % to 72 % and a concomitant increase in the

**FIG. 5** Two sections of the as-irradiated Zircaloy-4 cladding showing the hydride microstructure.

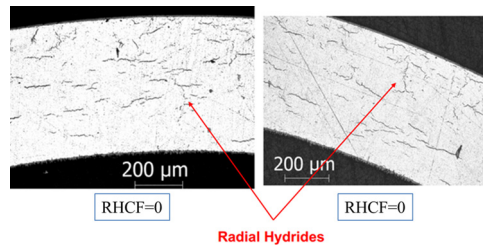
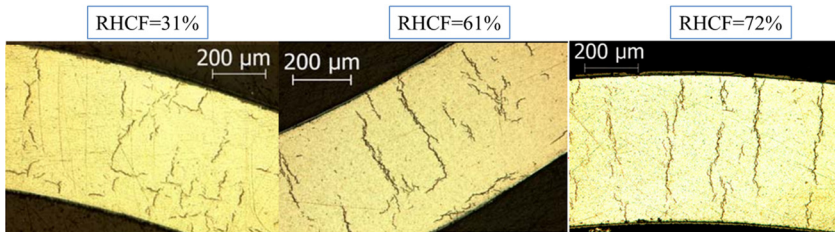


<sup>8</sup>RHCF is the ratio of the maximum length of the continuous radial and circumferential hydrides in a 150- $\mu\text{m}$  segment of the cladding divided by the thickness of the cladding. For a detailed explanation, see Billone, Burtseva, and Einziger [8].

**TABLE 1** List of M5 cladding samples tested.

Samples (ANL Designation)	Hydrogen Content (wt. ppm)	Oxide Thickness ( $\mu\text{m}$ )	Burnup (GWd/MTU)	Stress During Treatment (MPa)	RHCF after Treatment (%)
1 (652E6J)	$76 \pm 5$	8	72	0	0
2 (651E3H)	$58 \pm 15$	9	68	90	$31 \pm 13$
3 (651E5F)	$72 \pm 10$	8	68	110	$61 \pm 10$
4 (645D5)	$94 \pm 4$	13	63	140	$72 \pm 10$
5 (nonirradiated)	0	0	0	0	0

*Note:* The samples were heated to 400°C for 1 h and then cooled to 200°C with a rate of 5°C/min and finally cooled down to ambient temperature at the furnace cooling rate. Samples 2–4 were subjected to a one-cycle thermomechanical treatment. RHCF = radial hydride continuity factor.

**FIG. 6** The hydride microstructure of the as-irradiated M5 cladding material (Sample 1).**FIG. 7** Hydride microstructures of (a) Sample 2 with an RHCF of 31 %, (b) Sample 2 with an RHCF of 61 %, and (c) Sample 3 with an RHCF of 72 %. RHCF, radial hydride continuity factor.

radial hydride fraction from 10 % to nearly 100 % because most of the hydrides were aligned perpendicular to the hoop direction (Fig. 7c).

To examine the radioactive samples using synchrotron radiation diffraction, an encapsulating sample holder was designed to contain the sample using two layers of Kapton tape that were transparent to X-rays. The dose rates were measured as

2–5 mSv/h at 1 ft for  $\gamma$  only and 4–10 mSv/h at 1 ft for both  $\gamma$  and  $\beta$ , well below the APS limitations of 50 mSv/h at 1 ft as determined by the health physics division of the APS.

## Results and Discussion

### EFFECT OF STRESS STATE ON THE THRESHOLD STRESS FOR HYDRIDE REORIENTATION

To determine the effect of the stress state on the threshold stress for hydride reorientation, we (1) used the tapered uniaxial tensile specimen geometry (Fig. 1a) to determine the threshold stress ( $\sigma_1^{th}$ ) for the onset of hydride reorientation for a given thermomechanical treatment of Zircaloy-4 under uniaxial tension and (2) applied identical thermomechanical treatment to double-edge notched specimens with the geometries shown in Fig. 1b and c to determine the  $\sigma_1^{th}$  at different locations within the specimens with the use of the local stress states known at those locations from finite element analysis. All threshold stress values were determined from regions of the specimens that remained fully elastic and did not yield.

This approach relies on a light microscopy examination to determine the hydride microstructure coupled with stress analyses to determine the stress states at the locations where microscopy indicates a transition to out-of-plane hydride precipitation. Fig. 8 shows a cross sectional optical micrograph of a tapered uniaxial tension sample (Fig. 3a) after a two-cycle thermomechanical treatment for hydride reorientation. Because of the tapering, the tensile stresses varied along the length of the sample, thus allowing the  $\sigma_1^{th}$  value to be determined directly. The calculated tensile stress at the location for 0.05 RHF (155 MPa) was the  $\sigma_1^{th}$  for the transition from the in- to out-of-plane hydride precipitation. Above 177 MPa, the radial hydride fraction approached one, whereas it was zero below 145 MPa.

The threshold stress for hydride reorientation  $\sigma_1^{th}$  under biaxial stress states was assessed using a combination of metallographic examination and finite element analysis of the corresponding test specimens. Fig. 9 shows the results of one such

**FIG. 8** Hydride microstructure shown in a cross section of a tapered uniaxial tension sample along its edge plane after the two-cycle thermomechanical treatment shown in Fig. 2a. The threshold stress for hydride reorientation was approximately 155 MPa.

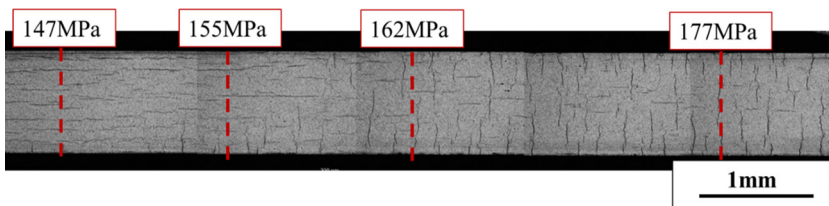
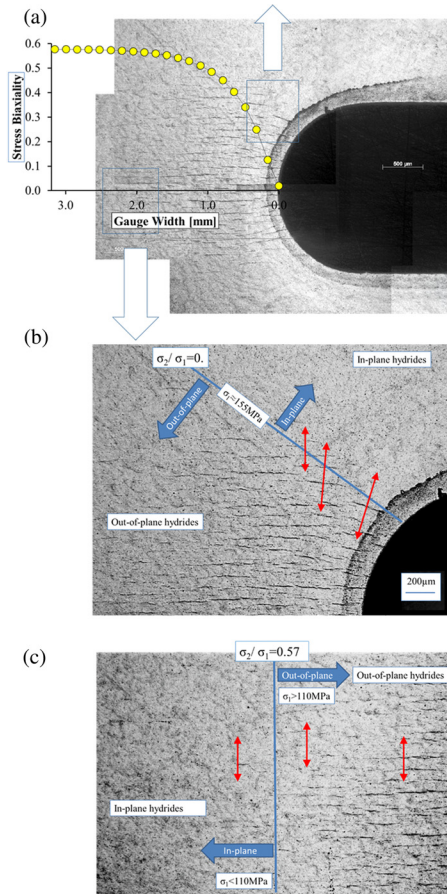


**FIG. 9** Optical micrographs showing an out-of-plane hydride microstructure within a double-edge notched plane-strain tensile specimen. (a) Radial hydride microstructure and stress biaxiality ratio ( $\sigma_2/\sigma_1$ ) across the gage section. At the applied stress used in this test, out-of-plane hydrides were visible in the uniaxial tensile region near the notch where the local value of the major stress exceeded 155 MPa (b). At a stress biaxiality ratio of 0.57 (c), the transition from in-plane to out-of-plane hydrides occurred at a maximum principal stress of 110 MPa. The red arrows in (b) and (c) show the orientations of the major stress at those locations.



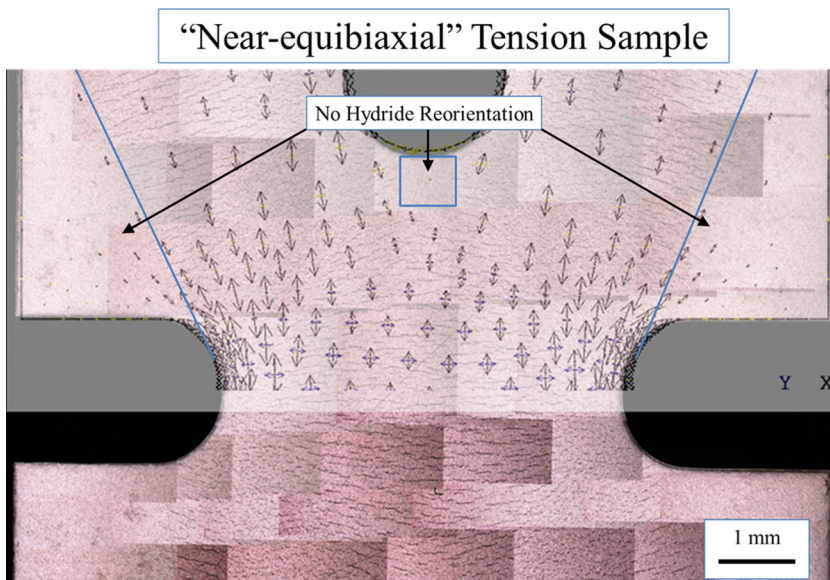
analysis for a plane-strain tension sample previously subjected to a two-cycle hydride reorientation treatment. As shown in Fig. 9a, the stress biaxiality ratio increases from 0 (uniaxial tension) near the notch to 0.57 (near plane strain) near the center of the gage section. Uniaxial tension conditions were present in many locations within the sample (such as along the strip of material near the edge of sample), which allowed us to estimate  $\sigma_1^{th}$  for the uniaxial tension as 155 MPa (Fig. 9b). It is significant that this  $\sigma_1^{th}$  value agreed with the value obtained from the

tapered uniaxial tension specimens shown in Fig. 8. At near plane-strain tension locations, examining regions such as the regions shown in Fig. 9b yields values of  $\sigma_1^{th} = 110 \pm 7$  MPa, much lower than for uniaxial tension.

Fig. 10 is an optical micrograph after testing showing the hydride microstructure with the major and minor stresses superimposed and with their respective orientations indicated. A careful analysis of the locations where  $\sigma_2/\sigma_1 = 0.83$  shows that for this condition  $\sigma_1^{th} = 75 \pm 10$  MPa. This threshold stress was significantly lower than the  $\sigma_1^{th}$  value in either uniaxial (155 MPa) or plane-strain tension (110 MPa). As expected, Fig. 10 shows that the out-of-plane hydrides were systematically oriented normal to the local major stress direction.

In the literature, threshold stresses for hydride reorientation in CWSR Zircaloy-4 samples subjected to uniaxial tension have been reported to be in the range of 140–200 MPa [22–24] with the exception of Chung et al. [47], who observed a value of 85 MPa. Thus, the  $\sigma_1^{th}$  values for uniaxial tension obtained in this study were in the range of previous measurements. For the plane-strain tension case,  $\sigma_1^{th}$  derived from thin-wall internally pressurized tubes ( $\sigma_2/\sigma_1 = 0.50$ ) ranged from 70 MPa for the un-irradiated Zircaloy-4 cladding samples (130–600 wt. ppm of hydrogen and treated from one to twelve cycles of thermomechanical treatment) [48] to 110 MPa for irradiated high-burnup (up to 55 GWD/t) pressurized water

**FIG. 10** An optical micrograph showing the hydride microstructure within a near-equibiaxial tension sample. The arrows show the orientations as well as the relative magnitudes of the major and minor stresses when a far-field stress is applied.



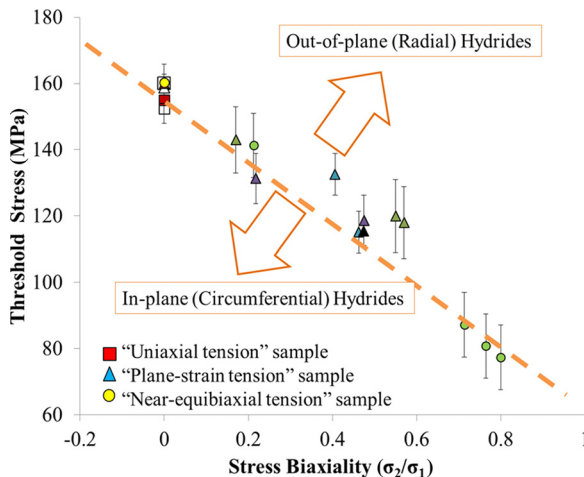
reactor cladding samples (30–110 wt. ppm hydrogen) for one-cycle treated samples [9]. Thus, the plane-strain threshold stress value of 110 MPa (at  $\sigma_2/\sigma_1 = 0.57$ ) observed herein was at the high end of previously reported internally pressurized tube test data for un-irradiated Zircaloy-4. These data also suggest that  $\sigma_1^{th}$  decreases with increasing stress biaxiality, as verified in Fig. 11.

The  $\sigma_1^{th}$  data as a function of biaxiality ratio are summarized in Fig. 11. A roughly linear decrease in threshold stress (major stress) was seen with an increasing stress biaxiality ratio. The net effect was that the threshold stress in near-equibiaxial tension was roughly half of that in uniaxial tension. It is significant that the  $\sigma_1^{th}$  values for uniaxial tension were determined from selected regions within all three specimen geometries (and from two different faces of the specimens), and the good agreement shown among the values for all types of samples supports the validity of the database.

### HYDRIDE DISSOLUTION/PRECIPITATION BEHAVIOR AND STRESS STATE

The previous section revealed an effect of the stress state on the hydride reorientation threshold stress in CWSR Zircaloy-4. Those results raise the question of whether there is also a significant effect of the stress state on the hydride structural response, as measured by the change in hydride lattice spacing, during dissolution/precipitation of both in- and out-of-plane hydrides in Zircaloy-4 during

**FIG. 11** The threshold stress (major stress) at the onset of radial hydride formation as a function of stress biaxiality for cold-worked stress-relieved Zircaloy-4 with a nominal 180 wt. ppm hydrogen and subjected to a two-cycle thermomechanical treatment. Each data point represents an average of three to five measurements. Error bars show the maximum and minimum values of threshold stress. Different colors indicate different individual samples, and different symbols indicate different sample types (each of which may contain regions with different states of stress).



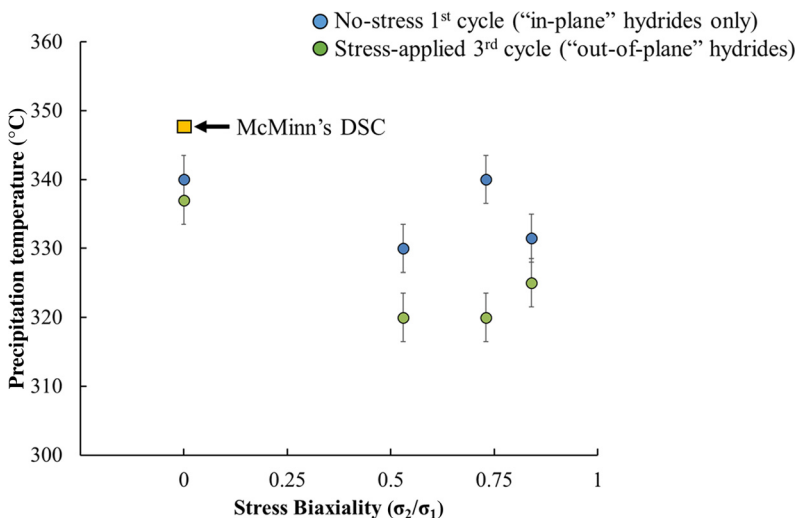
thermomechanical treatment. Synchrotron X-ray diffraction can be a useful technique for this purpose [22,39,41–44].

Because the intensity of diffraction signals associated with the  $\delta$ -hydride is related to the volume fraction of the corresponding phase, following the hydride intensity evolution during thermomechanical treatment it is possible to determine the hydride dissolution and precipitation temperatures in situ. The dissolution temperature  $T_d$  is the extrapolated temperature at which  $\delta$ -hydride intensity goes to zero during heating, whereas the precipitation temperature  $T_p$  is identified as the temperature at which hydride diffraction intensity reappears during cooling. In order to study the effect of the stress state on the hydride dissolution and precipitation temperatures while eliminating specimen-to-specimen variability, four different locations were measured within a single specimen.

The measured  $T_d$  values were very consistent, independent of stress state, and did not depend on whether in- or out-of-plane hydrides were dissolving. The values of  $T_d$  also agreed quite well with literature values of dissolution temperature, as determined by the diffusion coupling method [1] and differential scanning calorimetry [2].

Fig. 12 shows the values of  $T_p$  obtained from measurements at different locations with stress states from 0 to 0.83 within a single sample; data for in-plane hydrides (no stress, first cycle) as well as for out-of-plane hydrides (stress applied) are included. The  $T_p$  values for the in-plane hydrides that fell within the range of 330–340°C were consistent with literature values for  $T_p$  (310–347°C) [2,24] for this hydrogen

**FIG. 12** Precipitation temperature as a function of the stress biaxiality ratio for four different locations within a near-equibiaxial tension sample with a hydrogen content of 172 wt. ppm. The error bars were based on the maximum variation in the temperature measurement during the experiments. McMinn's data were acquired from the Zircaloy-4 weld material [2].

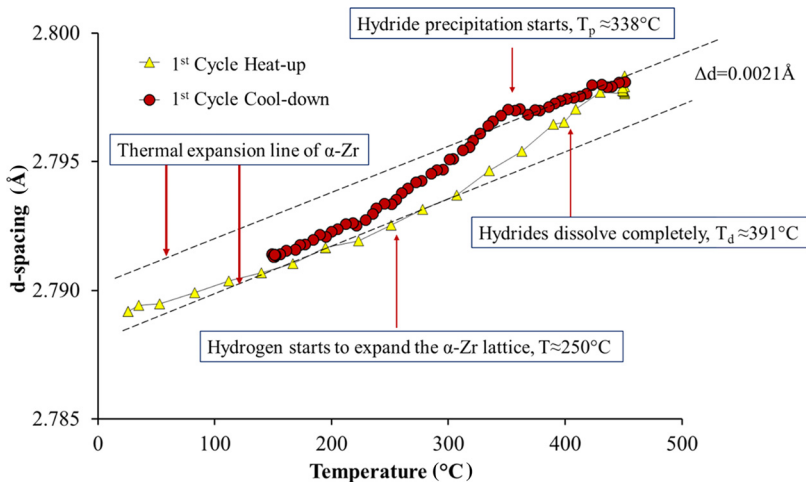


concentration. The precipitation temperatures for hydrides that precipitated under an applied stress (in these cases stresses above the reorientation threshold stress) were lower than for the hydrides that precipitated under no stress, suggesting that the precipitation temperature for reoriented hydrides is lower than that of in-plane hydrides. The effect would be consistent with the applied stress inhibiting the precipitation of in-plane hydrides, possibly by making it difficult for the usual orientation relation to be satisfied so that the precipitation has to happen under a different process and thus at lower temperatures. Moreover, the thermal history has an impact on the precipitation temperature such that the hydrides leave dislocation debris while dissolving in the parent zirconium [49]. Therefore, hydrides preferentially precipitate at those dislocation debris for the next cool-down cycle. Because the maximum temperature (450°C) in this study was too low for stress-relief anneal to occur, the maximum temperature and dwell time at the maximum temperature are expected to have minor effects.

### ZIRCONIUM MATRIX AND $\delta$ -HYDRIDE D-SPACING BEHAVIOR DURING THERMOMECHANICAL TREATMENT

The fitting of the  $\alpha$ -zirconium and  $\delta$ -hydride diffraction peaks yielded the peak positions that corresponded to the d-spacing in those phases. Because the measurement was done in situ, the detailed evolution of the d-spacings (and thus elastic strain) during the thermomechanical treatment can be followed. Fig. 13 shows the  $\alpha$ -zirconium {100} d-spacing evolution during the (stress-free) first cycle of the thermomechanical treatment shown in Fig. 3 and involving the dissolution and

**FIG. 13** The d-spacing variation of  $\alpha$ -zirconium {100} during one cycle of a stress-free thermomechanical treatment. The hydrogen content of this sample was 180 wt. ppm, and the cooling rate was 1°C/min. For clarity, not all data points are shown.



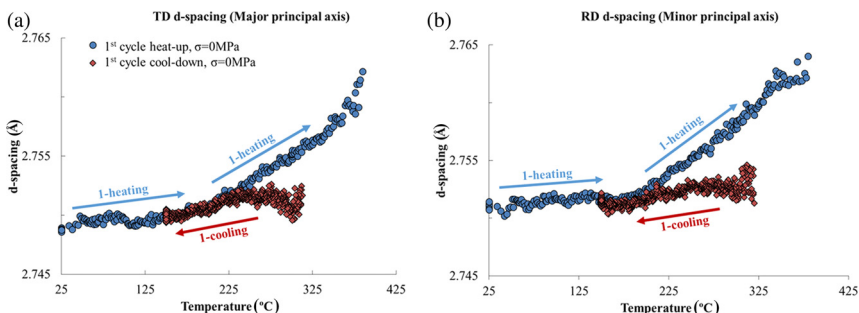


precipitation of in-plane hydrides. The  $\alpha$ -zirconium {100} d-spacing initially increased linearly with temperature at a rate of  $7.5 \times 10^{-6}/^\circ\text{C}$  (red triangles), similar to the Zircaloy-4 plate thermal expansion coefficient of  $7 \times 10^{-6}/^\circ\text{C}$  [41]. As the temperature approached  $250^\circ\text{C}$ , hydrogen atoms dissolved from the hydrides began to contribute to  $\alpha$ -zirconium d-spacing by expanding the zirconium lattice. When the hydride dissolution process was completed, the  $\alpha$ -zirconium d-spacing increase rate returned to its initial value (Fig. 13). These data are similar to previous studies [24,25,50] that also observed a similar lattice expansion during heating of hydrided Zircaloy. During cooling the same line was followed until hydride precipitation occurred, and when that finished ( $\sim 280^\circ\text{C}$ ) the lattice contraction rate reverted to the original value characteristic of the zirconium matrix. This value of the hydride precipitation temperature at which precipitation started ( $T_p$ ) and the dissolution temperature at which dissolution ended ( $T_d$ ) agreed well with the diffraction intensity determinations of  $T_d$  and  $T_p$  discussed previously.

It is also of great interest to study the d-spacing in the hydride particles, and for this we used the position of the strongest hydride diffraction peak (the  $\delta\{111\}$  peak). By integrating the diffraction rings over  $15^\circ$  segments of arcs aligned with the loading direction (TD) or normal to it (RD) [24,25], the hydride d-spacings could be independently tracked in the two sample directions. Note that for in-plane hydrides viewed as macroscopic platelets, both the TD and RD d-spacing data corresponded to  $\delta\{111\}$  planes aligned with the edges of the hydride platelets rather than with the hydride platelet faces.

Fig. 14a and b show the TD and RD d-spacing behavior of  $\delta\{111\}$  planes of in-plane hydrides during the first cycle. For temperatures up to approximately  $200^\circ\text{C}$ , the hydride planes along both TD and RD expanded at a rate ( $\sim 3 \times 10^{-6}/^\circ\text{C}$ ) that was somewhat less than that of the Zircaloy-4 matrix. However, at temperatures above  $200^\circ\text{C}$ , the d-spacing expansion rate increased to approximately  $20 \times 10^{-6}/^\circ\text{C}$

**FIG. 14** The evolution of  $\delta$ -hydride {111} d-spacing in (a) TD and (b) RD orientations during the first cycle of the thermomechanical treatment; no external stress was applied, and the microstructure consisted of in-plane hydrides. RD, rolling direction; TD, transverse direction.

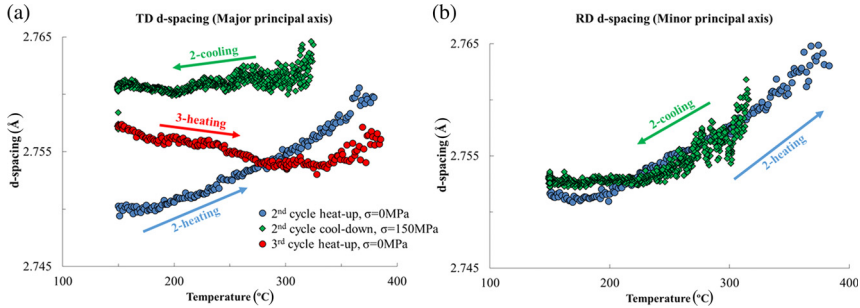


or roughly in between the thermal expansion coefficient of hydrides measured by Yamanaka et al. [51] ( $25\text{--}30 \times 10^{-6}/^{\circ}\text{C}$ ) and Beck ( $14.2 \times 10^{-6}/^{\circ}\text{C}$ ) [52]. Thus, the data show a two-stage bilinear thermal expansion behavior for hydride planes aligned with the platelet edges. Below  $200^{\circ}\text{C}$ , the hydride platelets were constrained to expand at a rate similar to that of the Zircaloy-4 matrix, whereas above  $200^{\circ}\text{C}$ , the matrix constraint appears to have decreased, allowing the hydride particles to expand at rates close to their own thermal expansion coefficient. It is important to note that subsequent cycles in which the precipitation under tensile stress induced out-of-plane hydrides only showed the bilinear thermal expansion behavior during heating for those  $\delta\{111\}$  planes aligned with the edges of the platelets (i.e., the RD data). Similar bilinear thermal expansion behavior has been observed previously for the  $\delta\{111\}$  planes aligned with the edges of hydride platelets in Zircaloy-4 [24,27,53]; in all cases, a higher thermal expansion rate was observed at elevated temperatures. No explanation has been offered for this effect to date.

Fig. 14 also shows that at the onset of in-plane hydride precipitation both the TD and RD  $\delta\{111\}$  d-spacings were lower than the value measured at the same temperature during heating, suggesting that the hydrides were under compressive strains when precipitation began. The d-spacing difference was roughly that expected from compressive strains limited by the flow stress of Zircaloy-4 ( $\sim 315$  MPa at  $325\text{--}330^{\circ}\text{C}$ ) assuming the elastic modulus of the  $\delta$ -hydride as 98 GPa at approximately  $300^{\circ}\text{C}$  [54]. Finally, continued cooling constrained the hydride to contract in a manner that was dictated by the matrix. As a result, at approximately  $225^{\circ}\text{C}$ , the hydride d-spacing matched that of the original d-spacing measured during heat up, and further cooling caused the in-plane hydrides to contract at a rate similar to that seen during heating.

The hydride d-spacing behavior during thermomechanical treatment cycling differed significantly when stress was applied to cause hydride reorientation. Fig. 15 shows the d-spacing behavior based on the diffraction data aligned along the TD and RD directions during heating/cooling of the second and third cycles of the thermomechanical treatment. During the second cycle heat up, the d-spacing behaved much as the first cycle for both TD and RD orientations because the  $\{111\}$  d-spacing of in-plane hydrides showed bilinear expansion behavior upon heating from  $150^{\circ}\text{C}$ . For the second cycle cool down, the load (applied at  $375^{\circ}\text{C}$ , a temperature at which all hydrogen was still in the solid solution [1,2]) caused out-of-plane hydride precipitation to initiate. When the stress was applied and hydride reorientation occurred, a comparison of Fig. 15a and b shows that the d-spacing behavior determined in the TD orientation was quite different from that in the RD orientation. To understand the significance of the difference, it is important to recognize the orientations of the specimen, hydrides, and incoming X-ray beam. Once out-of-plane hydrides were formed, the diffraction data obtained from the TD orientation (parallel to the major stress axis) corresponded to the d-spacing of  $\delta\{111\}$  planes oriented parallel to the apparent platelet faces. In contrast, the RD signal still corresponded to the  $\delta\{111\}$  d-spacing of the planes aligned along the platelet edges. The

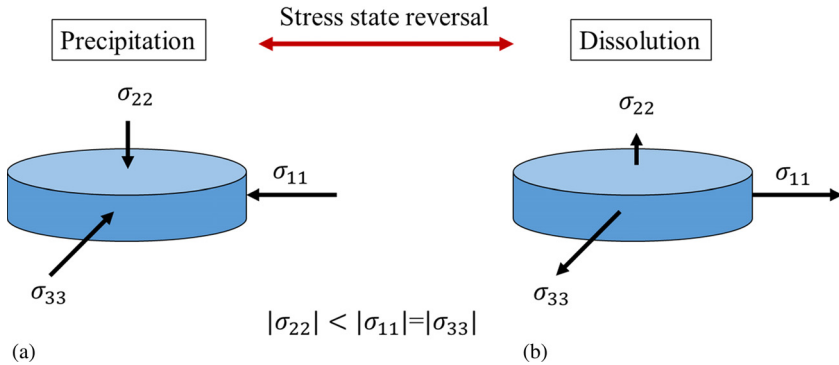
**FIG. 15** The  $\delta$ -hydride  $\{111\}$  d-spacing in (a) TD and (b) RD orientation during the thermomechanical cycling. Complete hydride reorientation occurred at the specific location, which was the center of the specimen where the major stress was 150 MPa and the stress biaxiality ratio was 0.53. The load was applied at 375°C during cooldown and removed at 150°C. RD, rolling direction; TD, transverse direction.



other factor was that the stress biaxiality ratio was  $\sigma_2/\sigma_1 = 0.57$ , which resulted in a near plane-strain condition.

The data in Fig. 15 can now be interpreted in terms of the strain behavior of face planes of the out-of-plane hydride platelets (i.e., the TD data) and the edge planes of the same platelets (i.e., the RD data). The cooling stage of the second cycle depicted the d-spacing behavior of out-of-plane hydride platelets forming and growing. Based on X-ray data generated at the RD orientation, Fig. 15b shows no large difference between the  $\delta\{111\}$  lattice plane spacing of in-plane hydrides (present during heating) and the corresponding d-spacing of out-of-plane hydrides that formed and grew during cooling of the subsequent cycles. Although the differences in d-spacing behavior shown in Fig. 16a (TD orientation) and b (RD orientation) are striking, it must be recalled that the RD data indicated  $\{111\}$  lattice spacing of those planes aligned with the platelet edges regardless of whether the hydrides were in plane or out of plane. Another factor in understanding the results is the fact that the RD orientation was aligned with the plane-strain direction of the loading used to reorient the hydrides. As a result, the application of a far-field load to precipitate out-of-plane hydrides did not cause an increase in d-spacing as determined in the RD orientation. Furthermore, the reorientation of the hydrides did not affect the d-spacing behavior of the  $\{111\}$  planes aligned with the platelet edges, although the hydrides were completely reoriented to the out-of-plane configuration at the end of the third cycle. Thus, the expansion/contraction behavior within the plane of the hydride platelet during heating/cooling was much like the first cycle response and even during subsequent thermomechanical treatment cycling. For the  $\{111\}$  d-spacing of those planes aligned with the platelet edges, bilinear thermal expansion behavior continued to exist upon heating, as is evident in the truncated data shown in Fig. 15b.

**FIG. 16** A schematic depiction of (a) the anisotropic triaxial stress state within the precipitated hydride platelet and (b) the resulting strain state within the platelet.



In contrast to the d-spacing behavior of  $\{111\}$  planes aligned with the platelet edges, the face planes showed much different behavior. Initially, with the load applied, there was significantly greater d-spacing among the face planes than that observed for the edge planes during either the previous heating cycle (Fig. 15a) or the concurrent cooling cycle (Fig. 15a and 15b). The d-spacing values for the planes parallel to the hydride faces (TD data) were higher than those aligned with the hydride edges (RD data). This disparity in spacing that occurred between those  $\delta\{111\}$  planes oriented parallel to the platelet faces (i.e., face planes) and those  $\delta\{111\}$  planes aligned with platelet edges (edge planes) was retained even after the load was removed at 150°C. Thus, with load removal at 150°C, the d-spacings in the precipitated hydride platelet were such that the face planes had 0.22 % greater spacing than the edge planes. This effect has been observed previously and referred to as the radial hydride signature [24]. Note that the same condition for the hydride strain state has also been observed by others for the in-plane hydrides, namely that the hydride face d-spacing is greater than the edge d-spacing [27]. Nearly identical behavior has been observed in the TD orientation d-spacing response during subsequent cycling (through five cycles). Thus, this hydride reorientation signature persists after many cycles and is retained after cooling to room temperature.

Fig. 15a also shows that the face-plane d-spacing data had the surprising behavior in that upon heating during the third cycle this particular  $\delta\{111\}$  spacing decreased with increasing temperatures. This anisotropic thermally induced contraction (the edge-aligned planes behaved normally) continued within the out-of-plane hydrides to a temperature of approximately 325°C, after which the d-spacing began to increase in a normal manner at a rate roughly equal to that of the thermal expansion rate of hydrides. This thermally induced contraction effect was also reproduced during several cycles of the thermomechanical treatment, although the cooling rates were faster

for the fourth (5°C/min) and fifth cycles (10°C/min) [55]. Although the data were not as complete, a similar d-spacing contraction effect has been observed for radial hydrides during a single heating cycle of a thermomechanical treatment of a Zr2.5Nb pressure tube containing 67 wt. ppm. hydrogen and loaded in uniaxial tension [28]. Examining the precipitation/dissolution behavior of hydrides in recrystallized Zircaloy-4 plates containing approximately 200 wt. ppm. hydrogen, Santisteban et al. [27] also observed a hydride d-spacing contraction during a single heating cycle. This latter observation is particularly significant because it was based on the d-spacing response of in-plane hydrides (not out-of-plane hydrides as in the present results) but with the diffraction condition such that the d-spacings of {111} planes determined were those of planes oriented parallel to the faces of the in-plane hydride platelets.

Santisteban et al. [27] also indicated that for in-plane hydrides there is also a {111} d-spacing disparity between those {111} planes parallel with the face of the hydride platelet and those {111} planes aligned with platelet edges: namely, similar to our observations for out-of-plane hydrides, their data for in-plane hydrides showed  $d_{\text{face planes}} > d_{\text{edge planes}}$ . Thus, we conclude that the following condition exists for both in- and out-of-plane hydrides in Zircaloy-4:  $d_{\text{face planes}} > d_{\text{edge planes}}$ .

#### **ANALYSIS OF $\delta$ -HYDRIDE D-SPACING BEHAVIOR DURING THERMOMECHANICAL CYCLING**

The complex behavior of the d-spacings of  $\delta\{111\}$  planes within the hydride platelets shown in Fig. 14 and Fig. 15 may be understood in terms of the stresses within the hydrides during dissolution upon heating and subsequent precipitation upon cooling. Although the hydrides on a microscopic level are believed to be constituted of many stacked hydride segments, their macroscopic shape is that of a thin plate with a large length/width ratio. For this discussion, we assume that the collective behavior of the individual microscopic hydrides is that of a macroscopically thin platelet embedded within the Zircaloy-4 matrix. The principal experimental results are as follows:

1. The d-spacings of the  $\delta\{111\}$  hydride planes oriented parallel with the face plane exceeded the spacing of those  $\delta\{111\}$  planes aligned to the edge of the platelet such that  $d_{\text{face planes}} > d_{\text{edge planes}}$ .
2. During heating/dissolution, the d-spacings of those  $\delta\{111\}$  planes aligned with the hydride plate edges exhibit a bilinear thermal expansion behavior. Upon heating, the d-spacings initially increase at rates ( $\sim 3 \times 10^{-6}/^\circ\text{C}$ ) close to that of the Zircaloy matrix, but above 200°C the expansion rate increased to roughly that of an unconstrained hydride ( $\sim 20 \times 10^{-6}/^\circ\text{C}$ ).
3. Upon heating/dissolution, the d-spacings of the  $\delta\{111\}$  planes oriented parallel to the hydride face initially contracted upon heating. This contraction continued until that d-spacing was similar to that of the  $\delta\{111\}$  planes aligned with the dissolving platelet edge.

To understand these experimental observations, the following is known regarding the stress state within the hydrides. Upon precipitation and owing to the transformation strain and (primarily) to the plate-like shape of the hydrides, the internal stresses within the precipitated hydrides are compressive such that the in-plane

stress components exceed the stress component normal to the platelet, as shown in Fig. 16. As described below, the resulting strain state is such that the d-spacing of planes parallel to the hydride face exceeds the spacing of those planes aligned with the plate edges within the precipitated hydrides. Recognized by Leitch and Shi [59] and estimated by Singh et al. [56], the dissolution of the hydrides quickly relaxes the compressive stresses and generates tensile stresses within the hydrides when those regions are converted back to the matrix.

To demonstrate the implications of these premises to our results, we applied the finite element analysis of Singh et al. [56] in which the stress field of a precipitating hydride platelet was computed based on a zirconium-hydrogen solid-solution matrix and a plate-like hydride with elastic/plastic properties. The basis for the analysis was the recognition of a large volume increase (17 %) associated with the transformation of the  $\alpha$ -zirconium solid solution to  $\delta$ -hydride and that the magnitudes of the transformation strain components are anisotropic, such that the two in-plane strain components have values of 4.6 % (at room temperature) but a much larger strain normal to the platelet (7.2 % at room temperature) [57,58]. In view of the above, a precipitating hydride plate would be expected to be under a state of triaxial compressive stresses that would reverse to tensile during dissolution. The elastic/plastic analysis of Singh et al. [56] extended an earlier analysis by Leitch and Puls [59] and took into account temperature-dependent hydride transformation strains, hydride moduli, and yield and matrix yield strengths. For the fully constrained case of an axisymmetric hydride platelet embedded in a zirconium-hydrogen matrix with temperature-dependent yield strengths (somewhat lower than those of the current Zircaloy-4 sheet), the analysis predicts an out-of-plane stress ( $\sigma_{22}$ ) and in-plane stresses ( $\sigma_{11} = \sigma_{33}$ ) that depend on whether the hydride is precipitating/expanding or dissolving/contracting [56]. It is important to note that the hydride stresses change from triaxial compression during precipitation to triaxial during dissolution, although the magnitude of these reversed tensile stresses will depend on the underlying assumptions of the details of the dissolution mechanism. Furthermore, as schematically illustrated in Fig. 16, the absolute magnitude of the in-plane stresses exceeds that of the stress normal to the hydride face.

The implications of the stress analysis may now be applied to understand the previously described d-spacing characteristics within the hydrides. Assuming isotropic elasticity within the hydride, the multiaxial stresses create spacing strains that can be calculated from

$$\epsilon_{11} = 1/[E(\sigma_{11} - \nu(\sigma_{22} + \sigma_{33}))] \quad (2)$$

where:

$\nu$  = Poisson's ratio, assumed to be  $1/3$ , and

$E$  = elastic modulus of the hydride, assumed to be equal to 87,000 MPa at 200°C and 97,000 MPa at room temperature [56,60].

In order to use Eq 2 to estimate the difference in d-spacings between  $\{111\}$  planes parallel to the hydride face and those  $\{111\}$  planes aligned with the plate

edges, the average values of the  $\sigma_{11}$  and  $\sigma_{22}$  stress components within the length of a hydride were estimated using data from Singh et al. [56] (Table 2). It should be recognized that the stress components listed in Table 2 generate equivalent stresses that obey the assumed hydride yield stress at the appropriate temperature [56]. However, the high room temperature yield stress assumed for the hydride results in very high predicted values of the stress components (especially  $\sigma_{11} = \sigma_{33}$ ) that will likely be reduced by plastic relaxation. In summary, Table 2 shows that the hydrides are subjected to triaxial compressive stresses but with the absolute magnitudes of the in-plane stresses exceeding those normal to the plane of the hydride plate (Fig. 16a).

Based on Eq 2 and the estimated average stresses within the hydrides, Table 2 compares the predicted hydride strains with those determined experimentally based on the  $\{111\}$  d-spacings within the precipitated hydrides. Agreement is reasonably good except at room temperature, where the predicted d-spacing strain was much larger than the observed value; in this case, the d-spacing measurements were made several hours after hydride reorientation occurred, and it is likely that plastic relaxation would have occurred, thereby reducing the  $(\Delta d/d)_{\text{obs}}$  value. The important point we wish to make is that the stress state within the precipitated hydrides was such that  $d_{\text{face planes}} > d_{\text{edge planes}}$ , and the scale of the observed difference was roughly that predicted by the simplified model.

As experimentally observed, the previously discussed analysis predicts that hydrides precipitate within Zircaloy with anisotropic d-spacings such that the  $\delta\{111\}$  planes oriented parallel with the face plane exceed the spacing of those  $\delta\{111\}$  planes aligned to the edge of the platelet. The hydrides are subjected to triaxial compressive stresses but with the absolute magnitudes of the in-plane stresses exceeding those normal to the plane of the hydride plate (Fig. 16a). Thus, a radial hydride signature only exists when comparing  $\delta\{111\}$  d-spacings of hydride face planes to those of edge planes.

The second principal experimental observation relates to the bilinear thermal expansion of  $\{111\}$  hydride planes oriented with the hydride plate edges. The triaxial compressive stress state acting on precipitated hydrides (Fig. 16a) constrains their

**TABLE 2** A comparison of observed and predicted strains based on  $\delta\{111\}$  d-spacing aligned with the hydride precipitate face and those planes aligned with plate edges.

Hydride	Temperature (°C)	$\sigma_{22}$ (MPa)	$\sigma_{11} = \sigma_{33}$ (MPa)	$(\Delta d/d)_{\text{pred}}$ (%)	$(\Delta d/d)_{\text{obs}}$ (%)
Out of plane	27	-420	-1,005	+0.88	0.29
Out of plane	200	-375	-560	+0.22	+0.22 at 150°C
In plane [27]	200	-375	-560	+0.22	+0.29 at 150°C

Note: The  $\sigma_{11}$ ,  $\sigma_{22}$ , and  $\sigma_{33}$  values are estimated averages over the width of the plate;  $\Delta d/d = (d_{\text{face}} - d_{\text{edge}})/d$ , where  $d_{\text{face}}$  is the  $\delta\{111\}$  d-spacing of planes aligned with the platelet face,  $d_{\text{edge}}$  is the corresponding d-spacing of planes aligned with the platelet edge, and  $d = (d_{\text{face}} + d_{\text{edge}})/2$ . The average values of  $\sigma_{11} = \sigma_{33}$  were obtained from  $\sigma_{11} = (3\sigma_m - \sigma_{22})/2$  [55].

expansion upon heating at low temperatures as long as no dissolution occurs; initial thermal expansion is thus similar to that of the Zircaloy matrix. However, above approximately 200°C, hydride dissolution initiates, and the resulting stress reversal causes tensile stresses in the plane of the hydride, as illustrated in Fig. 16b. These in-plane tensile stresses, which are especially pronounced near the perimeter of the hydride, enable the hydride to expand within its plane with minimal constraint and at roughly its inherent thermal expansion rate of an unconstrained hydride ( $\sim 20 \times 10^{-6}/^{\circ}\text{C}$ ). The result is bilinear thermal expansion of the hydride within its plane once dissolution initiates.

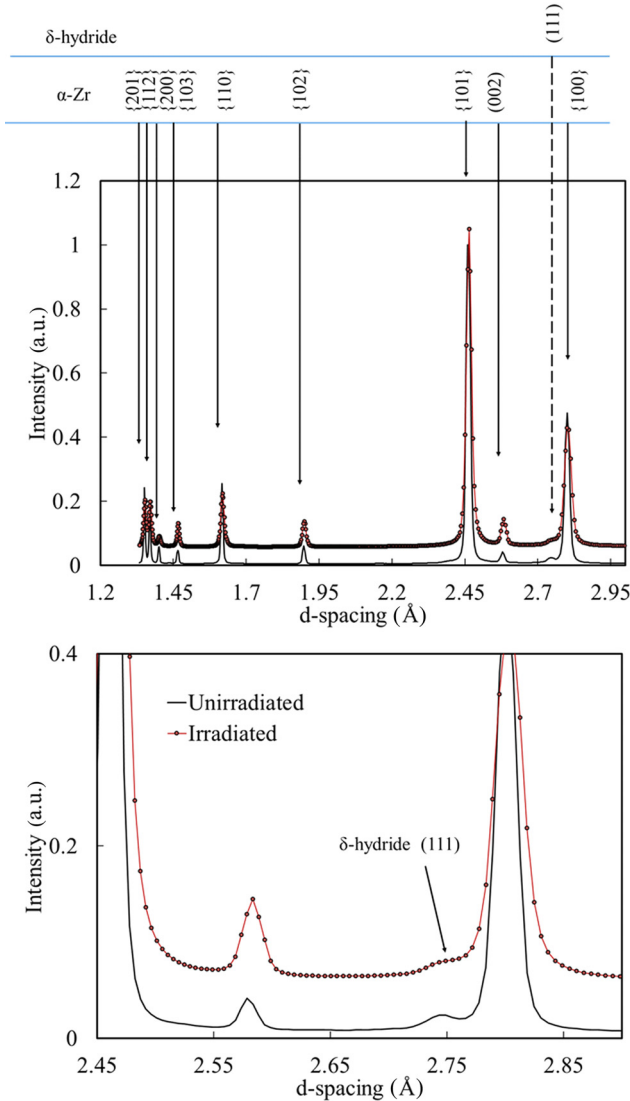
The final observation is related to the thermal contraction that occurs upon heating in the d-spacings of those  $\delta\{111\}$  planes aligned with the platelet face. In this study, the effect was observed with out-of-plane hydrides that formed under external stress such that the newly formed hydrides were thus subjected to the anisotropic stress state that results in  $d_{\text{face planes}} > d_{\text{edge planes}}$  (Table 2). According to the analyses [56,59], once hydride dissolution begins, a stress reversal occurs such that tensile stresses are created within the dissolving hydride. Thus, upon heating, the relaxation of the constraints due to the stress reversal causes the thermal contraction of the face planes within the hydride, enabling the d-spacing of the hydride to revert to an isotropic d-spacing value:  $d_{\text{face planes}} = d_{\text{edge planes}}$ . In other words, the observed thermally induced contraction of  $\{111\}$  planes aligned with the hydride platelet faces is also a result of dissolution relaxing the compressive stresses that caused the anisotropic d-spacing for those planes in the first place.

### X-RAY DIFFRACTION EXPERIMENTS OF IRRADIATED CLADDING TUBE SAMPLES

To further understand hydride reorientation, we performed X-ray diffraction experiments of the irradiated samples at ambient temperatures, as shown in Table 1. Thus, this section provides the X-ray diffraction signature of irradiated samples and experimental observations. Fig. 17 shows the diffraction patterns obtained for the irradiated Zircaloy-4 samples. The strongest  $\delta$ -hydride peak  $\{111\}$  was convoluted with an  $\alpha$ - $\{100\}$  zirconium peak as shown in Fig. 17, and the resulting d-spacings were calculated. When compared to the Powder Diffraction Files (05-0995 and 34-0649) [61], the peak positions corresponded quite well. The discrepancy was less than 0.15 %. As expected, the intensity of the observed peaks differed significantly from the powder diffraction data due to the crystallographic texture of the cladding tube. In particular, the intensity of the basal plane reflection was low since a majority of the basal planes have their normal parallel to the beam direction (radial direction of the tube). The diffraction pattern from the irradiated Zircaloy-4 cladding also shows wider  $\alpha$ -zirconium diffraction peaks, likely as a result of radiation damage. Neutron irradiation of zirconium alloys at reactor operating temperatures is known to result in the formation of dislocation loops, increasing peak broadening. Finally, the  $\delta\{111\}$  hydride peak was seen in both irradiated and un-irradiated Zircaloy-4, with similar d-spacings of 2.760 and 2.759 Å (irradiated) [61].

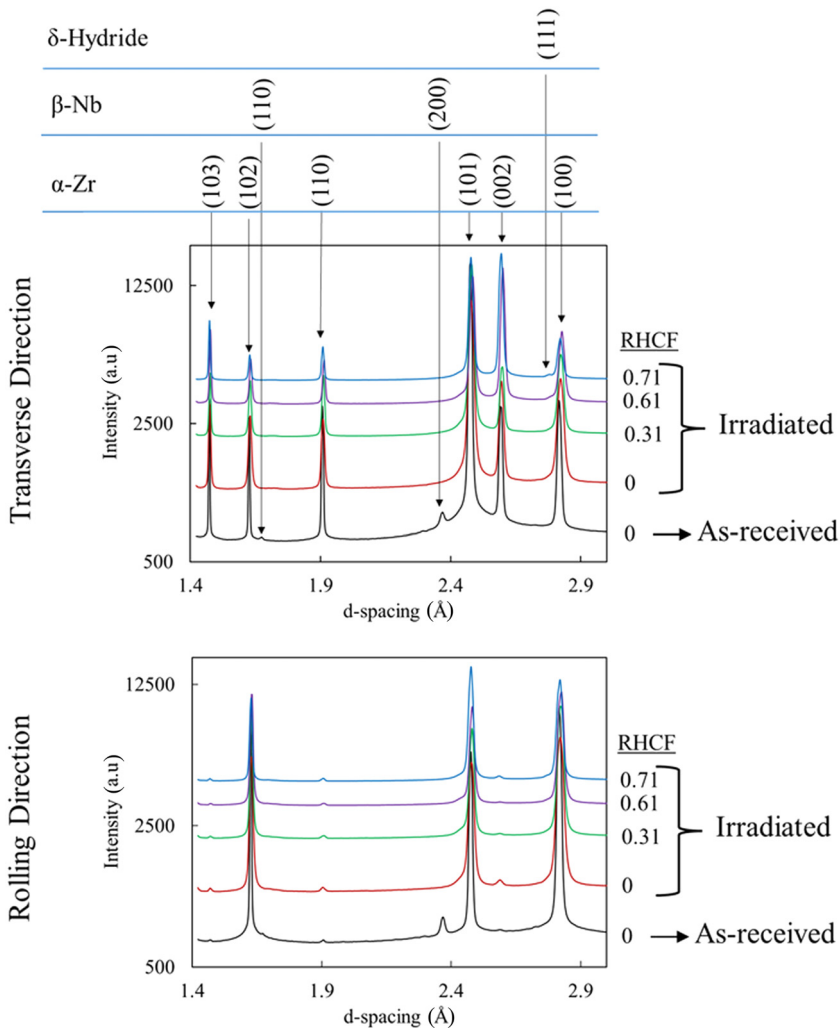


**FIG. 17** (a) X-ray diffraction pattern of both Zircaloy-4 irradiated tubing and an un-irradiated Zircaloy-4 sheet. (b) Magnified view of X-ray diffraction pattern shown in (a) in the region near the hydride peak. The  $\delta$ -hydride {220} and {200} peaks, having low intensity, were highly convoluted with  $\alpha$ -zirconium peaks and not indicated in this figure.



The X-ray diffraction patterns of the M5 cladding tube samples were also indexed for the hoop (transverse) and axial (rolling) directions [61], as shown in Fig. 18. In the un-irradiated sample, in addition to  $\alpha$ -zirconium peaks,  $\beta$ -niobium peaks were also observed as expected. Fig. 18 also shows a comparison of the X-ray diffraction of as-irradiated and the as-received M5 cladding tubes where an increase of the full width at half maximum in the  $\alpha$ -zirconium peaks in the irradiated

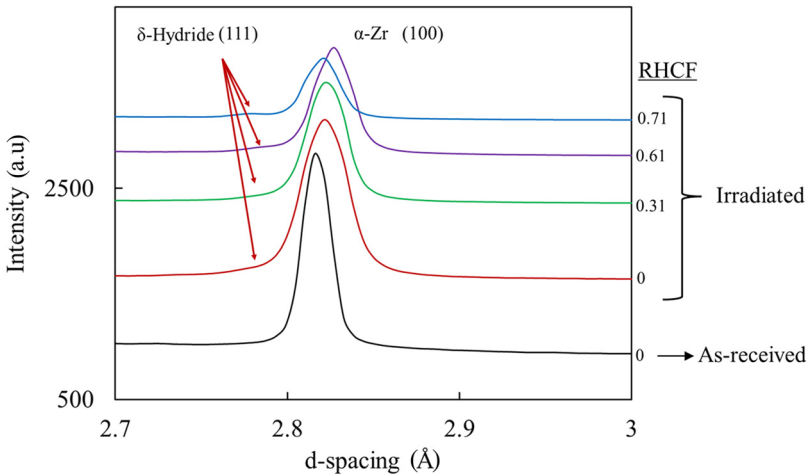
**FIG. 18** Comparison of the X-ray diffraction patterns of M5 un-irradiated, as-irradiated, and after different heat treatments causing the values of the radial hydride continuity factors to range from 0 to 0.71.



samples was apparent, as shown in Fig. 19. The main focus of this section was the determination of reoriented hydride peaks, but hydride peaks were not determined for both directions during diffraction tests of the irradiated samples. A notable result was that the  $\beta$ -phase peaks were no longer observable in the irradiated sample, indicating that the  $\beta$ -niobium phase had been modified by irradiation during reactor operation.

The most notable change in the diffraction patterns of the as-received state compared with the as-irradiated state was the significant decrease or disappearance of two  $\beta\{110\}$  and  $\{200\}$  niobium peaks that were visible before irradiation. This behavior was observed in the X-ray diffraction patterns of both circumferential and axial directions. For the as-irradiated samples, small diffuse shoulders near  $\alpha\{101\}$  and  $\alpha\{102\}$  zirconium peaks were observed near the expected  $\beta$ -niobium peak locations ( $\sim 2.4 \text{ \AA}$ ), i.e., a slightly large d-spacing than that of the initially observed  $\beta$ -niobium. This effect could have been caused by the dissolution of the  $\beta$  phase with the migration of niobium atoms into the  $\alpha$ -zirconium phase and the precipitation as small  $\beta$ -niobium-rich precipitates of different lattice spacing. Bechade et al. [62] observed the formation of nanometer-sized, needle-shaped, niobium-rich precipitates after the irradiation of M5.

**FIG. 19** The zoomed section of Fig. 18 that shows the expected  $\{111\}$  hydride peak locations and the increase in the full width at half maximum. Having low intensities due to the low hydrogen content of the specimen, the  $\delta$ -hydride  $\{220\}$  and  $\{200\}$  peaks were highly convoluted with  $\alpha$ -zirconium peaks and were not distinguishable.



## Conclusions

One main goal of this study was to investigate hydride reorientation in Zircaloy-4 under a multiaxial stress state. Mechanical test experiments were performed using a specially designed mechanical tensile test sample design that created a range of tensile biaxial stresses within the specimens. Matching the stress state calculated by finite element analysis at specific locations within a specimen local hydride microstructure made it possible to determine the threshold stress for hydride reorientation at different stress states. In situ high-energy X-ray diffraction experiments using synchrotron radiation were also performed to investigate the dissolution/precipitation behavior of both in- and out-of-plane (radial-type) hydrides during thermomechanical treatment. The major conclusions are as follows:

1. As the stress biaxiality ratio increases, the threshold stress for hydride reorientation decreases. The threshold stress (maximum principal stress) was determined to be 150 MPa for uniaxial tension, 110 MPa for plane-strain tension, and only 75 MPa for near-equibiaxial tension.
2. The d-spacing of the  $\delta\{111\}$  hydride planes parallel with the hydride platelet faces is higher than that of the hydride planes aligned with the platelet edges.
3. During heating, the d-spacings of those  $\delta\{111\}$  planes aligned with the hydride plate edges exhibit a bilinear thermal expansion, initially increasing at a rate close to that of the Zircaloy matrix, but above 200°C, close to that of the unconstrained hydride.
4. During heating/dissolution of the hydrides, the d-spacings of those  $\delta\{111\}$  planes oriented parallel to the hydride plate face initially contract upon heating. This contraction continues until that d-spacing is similar to that of the  $\delta\{111\}$  planes aligned with the dissolving platelet edge.
5. These d-spacing observations can be understood in a systematic manner by applying the finite element analysis of Singh et al. [56] that predicts anisotropic strains within the hydride such that  $d_{\text{face planes}} > d_{\text{edge planes}}$ . In addition, the stress state reversal predicted for hydride dissolution is consistent with the presence of both the bilinear thermal expansion of  $\delta\{111\}$  planes aligned with the platelet edges and the thermal contraction of those  $\delta\{111\}$  planes aligned with the platelet faces.
6. The investigation of hydride precipitation behavior using in situ synchrotron diffraction suggests that out-of-plane hydrides precipitate under stress at lower temperatures than in-plane hydrides, which precipitate under zero stress.
7. The examination of irradiated cladding using synchrotron radiation diffraction indicates that the  $\beta$ -niobium phase disappeared as a result of irradiation. Because of the low hydrogen contents of the irradiated samples, the hydride d-spacings could not be accurately determined.

From a technological point of view, these results indicate the importance of the stress state in assessing whether hydrides will reorient under engineering conditions such as vacuum drying of nuclear fuel rods.

## ACKNOWLEDGMENTS

This research was performed with funding from the Nuclear Regulatory Commission and used resources from the Advanced Photon Source under Contract No. DE-AC02-06CH11357. We thank our project manager Harold Scott for his support and helpful discussions.

## References

- [1] Kearns, J. J., "Terminal Solubility and Partitioning of Hydrogen in the Alpha Phase of Zirconium, Zircaloy-2 and Zircaloy-4," *J. Nucl. Mater.*, Vol. 22, No. 3, 1967, pp. 292-303.
- [2] McMinn, A., Darby, E. C., and Schofield, J. S., "The Terminal Solid Solubility of Hydrogen in Zirconium Alloys," *Zirconium in the Nuclear Industry: Twelfth International Symposium, ASTM STP1354*, G. P. Sabol and J. Moan, Eds., ASTM International, West Conshohocken, PA, 2000, pp. 173-195.
- [3] Kearns, J. J. and Woods, C. R., "Effect of Texture, Grain Size and Cold Work on the Precipitation of Oriented Hydrides in Zircaloy Tubing and Plate," *J. Nucl. Mater.*, Vol. 20, No. 3, 1966, pp. 241-261.
- [4] Louthan, M. R., Jr. and Marshall, R. P., "Control of Hydride Orientation in Zircaloy," *J. Nucl. Mater.*, Vol. 9, No. 2, 1963, pp. 170-184.
- [5] Ells, C. E., "Hydride Precipitates in Zirconium Alloys (A Review)," *J. Nucl. Mater.*, Vol. 28, No. 2, 1968, pp. 129-151.
- [6] Hardie, D. and Shanahan, M. W., "The Effect of Residual Stresses on Hydride Orientation in a Zirconium-2.5% Niobium Alloy," *J. Nucl. Mater.*, Vol. 50, No. 1, 1974, pp. 40-46.
- [7] Desquines, J., Cazalis, B., Bernaudat, C., Poussard, C., Averty, X., and Yvon, P., "Mechanical Properties of Zircaloy-4 PWR Fuel Cladding with Burnup 54-64MWd/kgU and Implications for RIA Behavior," *J. ASTM Int.*, Vol. 2, No. 6, 2005, pp. 1-20, <http://dx.doi.org/10.1520/JAI12465>
- [8] Billone, M., Burtseva, T., and Einziger, R., "Ductile-to-Brittle Transition Temperature for High-Burnup Cladding Alloys Exposed to Simulated Drying-Storage Conditions," *J. Nucl. Mater.*, Vol. 433, Nos. 1-3, 2013, pp. 431-448.
- [9] Aomi, M., Baba, T., Miyashita, T., Kamimura, K., Yasuda, T., Shinohara, Y., and Takeda, T., "Evaluation of Hydride Reorientation Behavior and Mechanical Properties for High-Burnup Fuel-Cladding Tubes in Interim Dry Storage," *J. ASTM Int.*, Vol. 5, No. 9, 2008, pp. 1-21, <http://dx.doi.org/10.1520/JAI101262>
- [10] Kubo, T., Kobayashi, Y., and Uchikoshi, H., "Determination of Fracture Strength of  $\delta$ -Zirconium Hydrides Embedded in Zirconium Matrix at High Temperatures," *J. Nucl. Mater.*, Vol. 435, Nos. 1-3, 2013, pp. 222-230.
- [11] Marshall, R. P., "Influence of Fabrication History on Stress-Oriented Hydrides in Zircaloy Tubing," *J. Nucl. Mater.*, Vol. 24, Nos. 1, 1967, pp. 34-48.
- [12] Sakamoto, K. and Nakatsuka, M., "Stress Reorientation of Hydrides in Recrystallized Zircaloy-2 Sheet," *J. Nucl. Sci. Technol.*, Vol. 43, No. 9, 2006, pp. 1136-1141.

- [13] Kiran Kumar, N. A. P., Szpunar, J. A., and He, Z., "Preferential Precipitation of Hydrides in Textured Zircaloy-4 Sheets," *J. Nucl. Mater.*, Vol. 403, Nos. 1-3, 2010, pp. 101-107.
- [14] Ells, C. E., "The Stress Orientation of Hydride in Zirconium Alloys," *J. Nucl. Mater.*, Vol. 35, No. 3, 1970, pp. 306-315.
- [15] Alam, A. M. and Hellwig, C., "Cladding Tube Deformation Test for Stress Reorientation of Hydrides," *J. ASTM Int.*, Vol. 5, No. 2, 2008, pp. 1-15, <http://dx.doi.org/10.1520/JAI101110>
- [16] Chu, H. C. C., Wu, S. K. K., Chien, K. F. F., and Kuo, R. C. C., "Effect of Radial Hydrides on the Axial and Hoop Mechanical Properties of Zircaloy-4 Cladding," *J. Nucl. Mater.*, Vol. 362, No. 1, 2007, pp. 93-103.
- [17] Singh, R. N., Lala Mikin, R., Dey, G. K., Sah, D. N., Batra, I. S., and Stähle, P., "Influence of Temperature on Threshold Stress for Reorientation of Hydrides and Residual Stress Variation across Thickness of Zr-2.5Nb Alloy Pressure Tube," *J. Nucl. Mater.*, Vol. 359, No. 3, 2006, pp. 208-219.
- [18] Min, S.-J., Won, J.-J., and Kim, K.-T., "Terminal Cool-Down Temperature-Dependent Hydride Reorientations in Zr-Nb Alloy Claddings under Dry Storage Conditions," *J. Nucl. Mater.*, Vol. 448, Nos. 1-3, 2014, pp. 172-183.
- [19] Desquines, J., Drouan, D., Billone, M., Puls, M. P., March, P., Fourceaud, S., Getrey, C., Elbaz, V., and Philippe, M., "Influence of Temperature and Hydrogen Content on Stress-Induced Radial Hydride Precipitation in Zircaloy-4 Cladding," *J. Nucl. Mater.*, Vol. 453, Nos. 1-3, 2014, pp. 131-150.
- [20] Hardie, D. and Shanahan, M. W., "Stress Reorientation of Hydrides in Zirconium-2.5% Niobium," *J. Nucl. Mater.*, Vol. 55, No. 1, 1975, pp. 1-13.
- [21] Daum, R. S., Majumdar, S., Liu, Y. Y., and Billone, M. C., "Radial-Hydride Embrittlement of High-Burnup Zircaloy-4 Fuel Cladding," *J. Nucl. Sci. Technol.*, Vol. 43, No. 9, 2006, pp. 1054-1067.
- [22] Bai, J. B., Ji, N., Gilbon, D., Prioul, C., and Francois, D., "Hydride Embrittlement in Zircaloy-4 Plate. Part II: Interaction Between the Tensile Stress and Hydride Morphology," *Metall. Mater. Trans. A*, Vol. 25A, No. 6, 1994, pp. 1199-1208.
- [23] Kese, K., *Hydride Re-Orientation in Zircaloy and Its Effect on the Tensile Properties*, Department of Materials Science and Engineering, Royal Institute of Technology, Stockholm, Sweden, 1998.
- [24] Colas, K. B., Motta, A. T., Daymond, M. R., and Almer, J. D., "Effect of Thermo-Mechanical Cycling on Zirconium Hydride Reorientation Studied In Situ with Synchrotron X-Ray Diffraction," *J. Nucl. Mater.*, Vol. 440, Nos. 1-3, 2013, pp. 586-595.
- [25] Colas, K. B., Motta, A. T., Almer, J. D., Daymond, M. R., Kerr, M., Banchik, A. D., Vizcaino, P., and Santisteban, J. R., "In Situ Study of Hydride Precipitation Kinetics and Re-Orientation in Zircaloy Using Synchrotron Radiation," *Acta Mater.*, Vol. 58, No. 20, 2010, pp. 6575-6583.
- [26] Blackmur, M. S., Robson, J. D., Preuss, M., Zanellato, O., Cernik, R. J., Shi, S.-Q., Ribeiro, F., and Andrieux, J., "Zirconium Hydride Precipitation Kinetics in Zircaloy-4 Observed with Synchrotron X-Ray Diffraction," *J. Nucl. Mater.*, Vol. 464, 2015, pp. 160-169.

- [27] Santisteban, J. R., Vicente-Alvarez, M. A., Vizcaino, P., Banchik, A. D., and Almer, J. D., "Hydride Precipitation and Stresses in Zircaloy-4 Observed by Synchrotron X-Ray Diffraction," *Acta Mater.*, Vol. 58, No. 20, 2010, pp. 6609–6618.
- [28] Vicente Alvarez, M. A., Santisteban, J. R., Vizcaino, P., Flores, A. V., Banchik, A. D., and Almer, J., "Hydride Reorientation in Zr2.5Nb Studied by Synchrotron X-Ray Diffraction," *Acta Mater.*, Vol. 60, No. 20, 2012, pp. 6892–6906.
- [29] Vicente Alvarez, M. A., Santisteban, J. R., Domizzi, G., and Almer, J., "Phase and Texture Analysis of a Hydride Blister in a Zr-2.5%Nb Tube by Synchrotron X-Ray Diffraction," *Acta Mater.*, Vol. 59, No. 5, 2011, pp. 2210–2220.
- [30] Vizcaino, P., Santisteban, J. R., Vicente Alvarez, M. A., Banchik, A. D., and Almer, J., "Effect of Crystallite Orientation and External Stress on Hydride Precipitation and Dissolution in Zr2.5%Nb," *J. Nucl. Mater.*, Vol. 447, Nos. 1–3, 2014, pp. 82–93.
- [31] Raynaud, P., Koss, D. A., Motta, A. T., and Chan, K. S., "Fracture Toughness of Hydrided Zircaloy-4 Sheet under Through-Thickness Crack Growth Conditions," *Zirconium in the Nuclear Industry: 15th International Symposium, ASTM STP1505*, B. Kammenzind and M. Limbäck, Eds., ASTM International, West Conshohocken, PA, 2007, pp. 163–177.
- [32] Tenckhoff, E., "Deformation Mechanisms, Texture, and Anisotropy in Zirconium and Zircaloy," *Zirconium in the Nuclear Industry, ASTM STP966*, ASTM International, West Conshohocken, PA, 1988, pp. 1–85.
- [33] Pierron, O. N., Koss, D. A., Motta, A. T., and Chan, K. S., "The Influence of Hydride Blisters on the Fracture of Zircaloy-4," *J. Nucl. Mater.*, Vol. 322, No. 1, 2003, pp. 21–35.
- [34] Delobelle, P., Robinet, P., Bouffiuou, P., Greyer, P., and LePichon, I., "A Unified Model to Describe the Anisotropic Viscoplastic Zircaloy-4 Cladding Tubes," *Zirconium in the Nuclear Industry: Eleventh International Symposium, ASTM STP1295*, E. R. Bradley and G. P. Sabol, Eds., ASTM International, West Conshohocken, PA, 1996, pp. 373–393.
- [35] Bickel, G., Green, L., James, M. W., Lamarche, T., Leeson, P., and Michel, H., "The Determination of Hydrogen and Deuterium in Zr-2.5Nb Material by Hot Vacuum Extraction Mass Spectrometry," *J. Nucl. Mater.*, Vol. 306, No. 1, 2002, pp. 21–29.
- [36] Raynaud, P. A., Koss, D. A., and Motta, A. T., "Crack Growth in the Through-Thickness Direction of Hydrided Thin-Wall Zircaloy Sheet," *J. Nucl. Mater.*, Vol. 420, Nos. 1–3, 2011, pp. 69–82.
- [37] Link, T. M., Koss, D. A., and Motta, A. T., "Failure of Zircaloy Cladding Under Transverse Plane-Strain Deformation," *Nucl. Eng. Des.*, Vol. 186, No. 3, 1998, pp. 379–394.
- [38] Pierron, O. N., Koss, D. A., and Motta, A. T., "Tensile Specimen Geometry and the Constitutive Behavior of Zircaloy-4," *J. Nucl. Mater.*, Vol. 312, Nos. 2–3, 2003, pp. 257–261.
- [39] Flanagan, M. E., "The Effect Of Hydrogen on the Deformation Behavior of Zircaloy-4," presented at *Water Reactor Fuel Performance Meeting*, Seoul, South Korea, October 19–23, 2008—unpublished.
- [40] Pierron, O. N., *Influence of Hydride Blisters on Failure of Zircaloy-4 Sheet*, Pennsylvania State University, State College, PA, 2002.

- [41] Siefken, L. J., Coryell, E. W., Harvego, E. A., and Hohorst, J. K., "MATPRO—A Library of Materials Properties for Light-Water-Reactor Accident Analysis," SCDAP/RELAP5/MOD 3.3 Code Manual, Vol. 4, Rev. 2, 2001.
- [42] Colas, K. B., Motta, A. T., Daymond, M. R., Almer, J. D., and Cai, Z., "Hydride Behavior in Zircaloy-4 during Thermomechanical Cycling," presented at *International Conference on Environmental Degradation of Materials in Nuclear Power Systems-Water Reactors*, Colorado Springs, CO, August 7, 2011, Wiley, Hoboken, NJ, 2012.
- [43] Larson, A. C. and Von Dreele, R. B., *General Structure Analysis System (GSAS)*, Los Alamos National Laboratory, Los Alamos, NM, 2000.
- [44] I. Seasolve Software, PeakFit Version 4.12, 2003.
- [45] Ruzauskas, E. J. and Fardell, K. N., *Design, Operation, and Performance Data for High Burnup PWR Fuel from H. B. Robinson Plant for Use in the NRC Experimental Program at Argonne National Laboratory*, Electric Power Research Institute, Palo Alto, CA, 2001.
- [46] Mitchell, D., Garde, A., and Davis, D., "Optimized ZIRLO Fuel Performance in Westinghouse PWRs," presented at *Top Fuel*, Orlando, FL, September 26–29, 2010—unpublished.
- [47] Chung, H. M., Daum, R. S., Hiller, J. M., and Billone, M. C., "Characteristics of Hydride Precipitation and Reorientation in Spent-Fuel Cladding," *Zirconium in the Nuclear Industry: Thirteenth International Symposium, ASTM STP1423*, G. D. Moan and P. Rudling, Eds., ASTM International, West Conshohocken, PA, 2002, pp. 561–582.
- [48] Chu, H. C., Wu, S. K., and Kuo, R. C., "Hydride Reorientation in Zircaloy-4 Cladding," *J. Nucl. Mater.*, Vol. 373, Nos. 1–3, 2008, pp. 319–327.
- [49] Carpenter, G. J. C. and Watters, J. F., "An In-Situ Study of the Dissolution of  $\gamma$ -Zirconium Hydride in Zirconium," *J. Nucl. Mater.*, Vol. 73, No. 2, 1978, pp. 190–197.
- [50] Colas, K. B., Motta, A. T., Daymond, M. R., Kerr, M., and Almer, J. D., "Hydride Platelet Reorientation in Zircaloy Studied with Synchrotron Radiation Diffraction," *J. ASTM Int.*, Vol. 8, No. 1, 2011, No. 1, pp. 1–17, <http://dx.doi.org/10.1520/JAI103033>
- [51] Yamanaka, S., Yoshioka, K., Uno, M., Katsura, M., Anada, H., Matsuda, T., and Kobayashi, S., "Thermal and Mechanical Properties of Zirconium Hydride," *J. Alloys Compd.*, Vols. 293–295, 1999, pp. 23–29.
- [52] Beck, R. L., "Zirconium-Hydrogen Phase System," *Trans. ASM.*, Vol. 55, No. 3, 1962, pp. 542–555.
- [53] Zanellato, O., Preuss, M., Buffiere, J.-Y., Ribeiro, F., Steuwer, A., Desquines, J., Andrieux, J., and Krebs, B., "Synchrotron Diffraction Study of Dissolution and Precipitation Kinetics of Hydrides in Zircaloy-4," *J. Nucl. Mater.*, Vol. 420, Nos. 1–3, 2012, pp. 537–547.
- [54] Rico, A., Martin-Rengel, M. A., Ruiz-Hervias, J. Rodriguez, J., and Gomez-Sanchez, F. J., "Nanoindentation Measurements of the Mechanical Properties of Zirconium Matrix and Hydrides in Unirradiated Pre-Hydrided Nuclear Fuel Cladding," *J. Nucl. Mater.*, Vol. 452, Nos. 1–3, 2014, pp. 69–76.
- [55] Cinbiz, M., *The Effect of Stress State on Zirconium Hydride Reorientation*, Pennsylvania State University, State College, PA, 2015.



- [56] Singh, R. N., Khandelwal, H. K., Bind, A. K., Sunil, S., and Stähle, P., "Influence of Stress Field of Expanding and Contracting Plate Shaped Precipitate on Hydride Embrittlement of Zr-Alloys," *Mater. Sci. Eng. A*, Vol. 579, 2013, pp. 157–163.
- [57] Carpenter, G. J. C., "The Dilatational Misfit of Zirconium Hydrides Precipitated in Zirconium," *J. Nucl. Mater.*, Vol. 48, No. 3, 1973, pp. 264–266.
- [58] Singh, R. N., Stähle, P., Massih, A. R., and Shmakov, A. A., "Temperature Dependence of Misfit Strains of  $\delta$ -Hydrides of Zirconium," *J. Alloys Compd.*, Vol. 436, Nos. 1–2, 2007, pp. 150–154.
- [59] Leitch, B. W. and Puls, M. P., "Finite Element Calculations of the Accommodation Energy of a Misfitting Precipitate in an Elastic-Plastic Matrix," *Metall. Trans. A*, Vol. 23A, No. 3, 1992, pp. 797–806.
- [60] Puls, M. P., "Hydrogen Induced Delayed Cracking: 2. Effect of Stress on Nucleation, Growth, and Coarsening of Zirconium Hydride Precipitates," AECL-8381, 1984, p. 30.
- [61] International Centre for Diffraction Data, Powder Diffraction File, 2006.
- [62] Béchade, J. L., Menut, D., Doriot, S., Schlutig, S., and Sitaud, B., "X-Ray Diffraction Analysis of Secondary Phases in Zirconium Alloys before and after Neutron Irradiation at the MARS Synchrotron Radiation Beamline," *J. Nucl. Mater.*, Vol. 437, Nos. 1–3, 2013, pp. 365–372.

## Discussion

*Question from Toyoshi Fuketa, Nuclear Regulation Authority, Japan:—*Aren't there any effects of hydrides on the stress condition? Don't hydrides affect the stress conditions?

*Authors' Response:—*In this study we considered only the stress state of the matrix. The effects of the hydride inclusions on the stress state were not considered because the hydride volume fraction was too low to affect the stress state of the matrix under mechanical load. (The maximum hydrogen content was 180 wt. ppm.) The hydrides were thereby reasonably well separated, and the matrix dominated the mechanical behavior.

*Question from Mirco Grosse, Karlsruhe Institute of Technology:—*You interpret the changes in d-spacing as being caused by stresses. Can changes in the stoichiometry also be the reason for the variation of the d-spacing?

*Authors' Response:—*Absolutely. This is another possibility as we point out in the paper. The stoichiometry effect on  $\delta$ -hydride d-spacing is presented by Singh et al. [1], based on the study of Yamanaka et al. [2]. As shown in Fig. 1, the increasing stoichiometry increases the lattice parameter of the  $\delta$ -hydrides, which also causes the  $\delta\{111\}$  d-spacing increase. In our study, we were not able to separate any stoichiometry change effects and mechanical loading during heat-up and cool-down cycles.

- [1] Singh, R. N., Khandelwal, H. K., Bind, A. K., Sunil, S., and Stähle, P., "Influence of Stress Field of Expanding and Contracting Plate Shaped Precipitate on Hydride Embrittlement of Zr-Alloys," *Mater. Sci. Eng. A*, Vol. 579, 2013, pp. 157–163.
- [2] Yamanaka, S., Yoshioka, K., Uno, M., Katsura, M., Anada, H., Matsuda, T., and Kobayashi, S., "Thermal and Mechanical Properties of Zirconium Hydride," *J. Alloys Compd.*, Vols. 293–295, 1999, pp. 23–29.